Hydrogen production from hydrolysis of magnesium wastes reprocessed by mechanical milling under air

María Rodríguez, Franco Niro, Guillermina Urretavizcaya, Jean-Louis Bobet, Facundo Castro

Hydrogen production from hydrolysis of magnesium wastes reprocessed by mechanical milling under air

María Rodríguez[a, b], Franco Niro[a, c], Guillermina Urretavizcaya[b, d], Jean-Louis Bobet[e], Facundo J. Castro[b, d]

[a]CNEA, Centro Atómico Bariloche, S. C. de Bariloche, Río Negro, Argentina
[b]Universidad Nacional de Cuyo, Instituto Balseiro, S. C. de Bariloche, Río Negro, Argentina
[c]Universidad Nacional de San Martín, Instituto Jorge A. Sábato, San Martín, Buenos Aires, Argentina
[d]CNEA, CONICET, Centro Atómico Bariloche, S. C. de Bariloche, Río Negro, Argentina
[e]University of Bordeaux, CNRS, Bordeaux INP, ICMCB, UMR 5026, F-33600, Pessac, France

Keywords: Hydrogen production, Hydrolysis, Magnesium waste, Mechanical milling

Abstract
Magnesium-based wastes were reprocessed by mechanical milling under air atmosphere and used to produce hydrogen by hydrolysis. The evolution of the material during reprocessing and the generation of hydrogen in a 0.6 M $MgCl_2$ aqueous solution at 24ºC are reported. The morphology, microstructure and phase abundance change with milling time. With mechanical processing particle size and crystallite size reduce, microdeformations accumulate in the material, Al dissolves in (Mg), the amount of $Mg_{17}Al_{12}$ (β-phase) increases and small quantities of Fe from the milling tools are incorporated in the material. Hydrogen yields in the 70-90% range after 30 minutes of reaction have been obtained, depending on particle size and milling time. Reactants are not exhausted during the hydrolysis reaction in the saline solution, due to the formation of a $Mg(OH)_2$ layer that produces a passivating effect. Higher generation has been observed for larger particles and for materials reprocessed for longer milling times. Reaction kinetics also improves with milling time, with faster rates observed for the smaller particles. The shape of the hydrolysis curves can be fitted with a model that corresponds to a reaction limited by a three dimensional geometric contraction process. $Mg_{17}Al_{12}$ and Fe favor hydrogen production by acting as micro-galvanic cathodes during the reaction.

1 Introduction

Hydrogen production is a very active research field [Nikolaidis 2017]. This is a consequence of hydrogen being an interesting option to replace the contemporary energy scheme based on fossil fuels [Mazloomi 2012, Abe 2019]. Currently, 95% of hydrogen is produced from fossil fuels, using established technologies like hydrocarbon reforming and pyrolysis, and the remaining 5% is obtained from water electrolysis [Nikolaidis 2017]. Alternative production methods based on renewables exist, and can be classified into two major categories: biomass processes and water splitting methods. The first category includes biological processes, as bio-photolysis, dark fermentation and photo fermentation, and the second one electrolysis, thermolysis and photolysis [Nikolaidis 2017]. Though these technologies are not yet mature to be globally implemented, it is expected that some of them would be operative in the near future, when fossil fuel substitution would be inevitable. In the near term, other technologies appear as interesting options for small scale appliances and low-energy consuming devices. One of them is hydrogen production from hydrolysis [Xu 2018, Marrero-Alfonso 2009].

The hydrolysis reaction of a metal *M* of groups 1, 2 or 13 of the periodic table can be represented by the reaction:

$$M\,(s) + nH_2O\,(l) \rightarrow M(OH)_n\,(s) + n/2\;H_2\,(g)$$

where *n* is the oxidation state of *M*.

The hydrides of these metals can also react with water or an aqueous solution to produce hydrogen by following the reaction:

$$MH_n\,(s) + nH_2O\,(l) \rightarrow M(OH)_n\,(s) + n\,H_2\,(g)$$

Additionally, complex chemical hydrides of light elements can also be used to produce H_2 by hydrolysis following a more complex route [Marrero-Alfonso 2009].

Among the light metals, Mg and its hydride MgH_2 stand out for hydrogen generation due to their high capacity (8.2 and 15.2 wt%, without taking into account the mass of water, respectively), their mild reaction conditions (room temperature and atmospheric pressure), the purity of the H_2 obtained, and the environmental safety of the $Mg(OH)_2$ obtained as a byproduct of the reaction [Liu 2021]. Another advantage of Mg is its increasing use in different applications [Prasad 2021] and the consequent availability of Mg wastes. Nowadays only high-grade Mg scraps are recycled, the low grade fraction remaining as environmental liabilities for techno-economic reasons. The use of these low-grade Mg wastes to produce H_2 has the double benefit of converting a pyrophoric dangerous waste like Mg into $Mg(OH)_2$ and simultaneously producing an environment-friendly fuel.

In the last years some efforts have been devoted to this task. Uan *et al.* have explored hydrogen production from low-grade Mg wastes with or without catalytic nets [Uan 2007, Uan 2009, Uan 2009b]. In [Uan 2007] they have reported the production of hydrogen from remelted Mg wastes in a NaCl solution using a Pt-coated Ti net that worked as a catalyst. During the experiment, the catalyst net was either statically loaded over the surface of the sample or ground against it. Their results have evidenced the effect of a passive $Mg(OH)_2$ layer formed on the surface that limits H_2 production. Effectively, when the catalyst net was statically loaded H_2 generation stopped after a certain time, but when the net was ground against the surface and the $Mg(OH)_2$ layer removed, H_2 production continued at a stationary rate. In [Uan 2009] they describe the use of a Pt-coated Ti net or a 304 stainless-steel net embedded in remelted low-grade Mg scraps. In both cases H_2 was produced at a steady rate when immersing the samples in a NaCl aqueous solution, but the samples prepared with the Pt-coated Ti net have produced a greater amount of H_2 per unit time. The differences have been interpreted considering the larger difference in electrochemical potential between Mg and Pt than that between Mg and steel. In [Uan 2009b] the addition of citric acid to natural seawater has allowed H_2 to be produced at satisfactory rates with or without embedded stainless-steel nets. Moreover, even as-received low-grade Mg wastes have produced H_2 at measurable rates. Figen *et al.* [Figen 2015, Figen 2 2015] have explored hydrogen generation using Mg wastes from a gold manufacturing factory. They have successfully produced H_2 after mechanical milling the wastes and found that the use of $NiCl_2$ solutions prepared with distilled water or sea water from Marmara Sea or Aegean Sea produces the best yields compared with $CoCl_2$, $CuCl_2$, $FeCl_3$ and $MnCl_2$ solutions. In an interesting paper, Matsuzaki et al. [Matsuzaki 2017] have produced H_2 from the hydrolysis of simulated Mg and AZ91 wastes during mechanical milling. Within a special milling chamber with a gas outlet, H_2 was generated during the milling process of Mg or AZ91 chips mixed with seawater. Greater amounts and faster rates have been observed for both materials when the hydrolysis was carried out during ball milling, compared with a stationary process. These improvements have been attributed to the removal of $Mg(OH)_2$ layers and the exposure of fresh surfaces during milling. Additionally, higher yields and faster rates have been recorded for Mg compared with AZ91, due to the better corrosion resistance of the commercial alloy. Recently, Al Bacha et al. [Al Bacha 2019, Al Bacha 2020, Al Bacha 2020 b] have studied H_2 production from

wastes of different Mg-based materials, such as WE43 commercial alloy [Al Bacha 2019] and scraps from the machining of sacrificial anodes [Al Bacha 2020, Al Bacha 2020 b]. In these works wastes have been processed by mechanical milling under inert (Ar) or reactive (H_2) atmospheres with or without additives like C (graphite), Ni and $AlCl_3$. In these articles the effect on the hydrolysis performance of different factors has been studied and analyzed. In particular, milling device (scale), milling time, milling atmosphere, the role of the additives, the effect of their combination and of its order of incorporation have been documented.

In this work we report some advances in the H_2 generation by hydrolysis of Mg wastes reprocessed by mechanical milling under air atmosphere and using no additives. This process has a clear economic and environmental advantage, as the need of using expensive inert or reactive gases is replaced by a cheaper processing under air. In the following we show that hydrogen yields between 70% and 90% are obtained after 30 minutes in a reaction controlled by a geometric contraction process. The influence on hydrogen production of: the properties of the reprocessed materials, the presence and proportion of different phases with catalytic effect, and the formation of a passivating $Mg(OH)_2$ layer are discussed.

2 Experimental

Chips from the manufacturing of sacrificial anodes were used as starting material (see Supplementary material, Fig. S1). By X-ray diffraction and EDS analysis the material has been found to be an inhomogeneous mixture of scraps of Mg alloys and chips of an Al alloy. The global composition has been estimated as a Mg content of 90 wt%, an approximate Mg/Al mass ratio of 10:1, and Zn, Cu, and Mn as minor components. Before milling, the chips were washed three times with acetone in an ultrasonic bath. Milling was done under air atmosphere in a Fritsch-Pulverisette P6 monomill at 400 rpm for 2, 5, 10 and 20 h using a ball to mass ratio 40:1. The milling schedule consisted of 10 minutes of milling followed by 20 minutes of rest, to avoid overheating. The milled materials were stored in an MBraun glovebox with O_2 and H_2O contents below 1ppm. Inside the glovebox the processed material was sorted into size ranges by using 100 μm and 200 μm sieves. Three sets of materials with the following dimensions were obtained: 1) less than 100 μm, 2) within a 100-200 μm range, and 3) greater than 200 μm. X-ray diffraction experiments were done using a Bruker D8 Advance instrument. Rietveld refinement of the data was done with Fullprof [Fullprof]. SEM and EDS characterization was made in a SEM FEI Inspect S50 equipment. Hydrolysis reaction was carried out in a custom made instrument described elsewhere [Pighin 2020]. Approximately 20 mg of material were hydrolyzed in 50 mL of a 0.6 M $MgCl_2$ aqueous solution at 24ºC, with temperature controlled by a thermal bath. During the reaction the solution was continuously stirred. When H_2 evolution had stopped, 10 mL of 0.5 M HCl were added to the system to complete the reaction.

3 Results and Discussion

3.1 Size distribution and morphology of the milled material

The initial size of the scraps is drastically reduced by mechanical milling (Fig. 1). After 2h of mechanical processing 76 wt% of the material passes the 100 μm sieve. Subsequent milling up to 5h produces a slight decrease in the amount of material with sizes below 100 μm, probably due to some agglomeration of the particles as a consequence of cold welding. By further milling up to 20h, the proportion that passes the 100 μm sieve increases, with 88 wt% of the material with sizes below 100 μm, and 9 wt% in the 100-200 μm range.

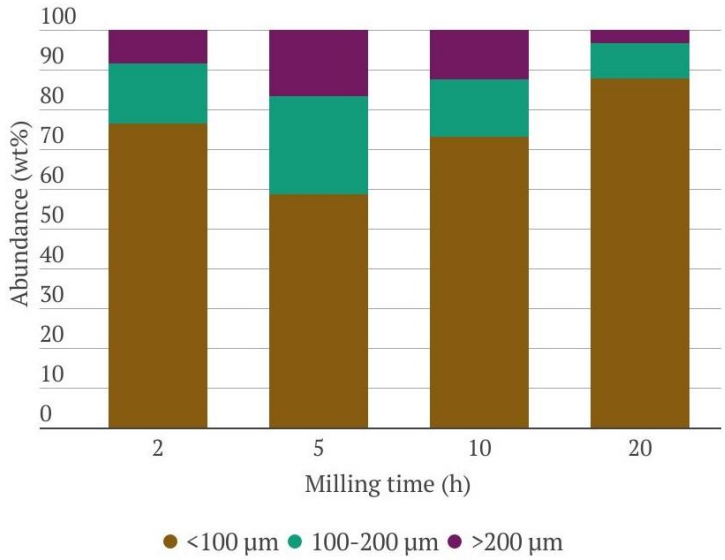

Fig. 1: Amount of milled material in the < 100 µm, 100-200 µm, and > 200 µm size ranges for the different milling times.

SEM images of the 100-200 µm size range (Fig. 2) show that particle size and morphology do not significantly change from 2 to 20 h of milling time for this size fraction. Compact agglomerates with parallel flat surfaces are observed at all milling times, probably as a consequence of the ductile character of the material. Only a slight increase in the separation of the flat surfaces (*i.e.* thickness) and the presence of more rounded agglomerates can be observed as milling time augments.

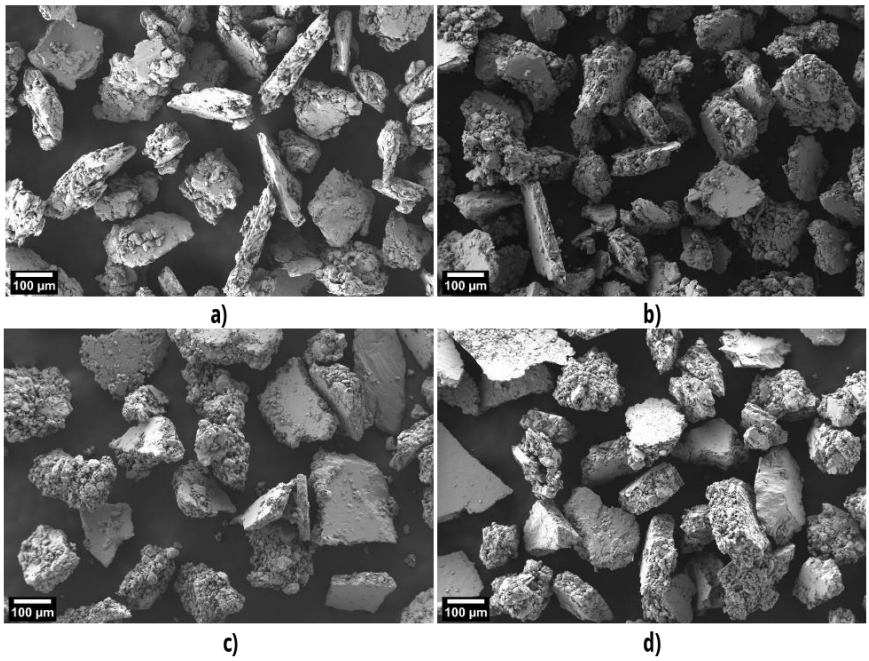

Fig. 2: SEM images of the material in the 100-200 µm size range after different milling times. a) 2h, b) 5h, c) 10h and d) 20h

The morphological features of the material that passes the 100 μm sieve (Fig. 3) are similar to those of the 100-200 μm size range agglomerates for the 2h- and 5h-milled materials. When milling extends to 10h and 20h, only a few of agglomerates with flat surfaces are found, and a noticeably reduction of size takes place. Particle size distribution seems to be less uniform in these materials, with small agglomerates of 10 μm coexisting with chunks of 100 μm.

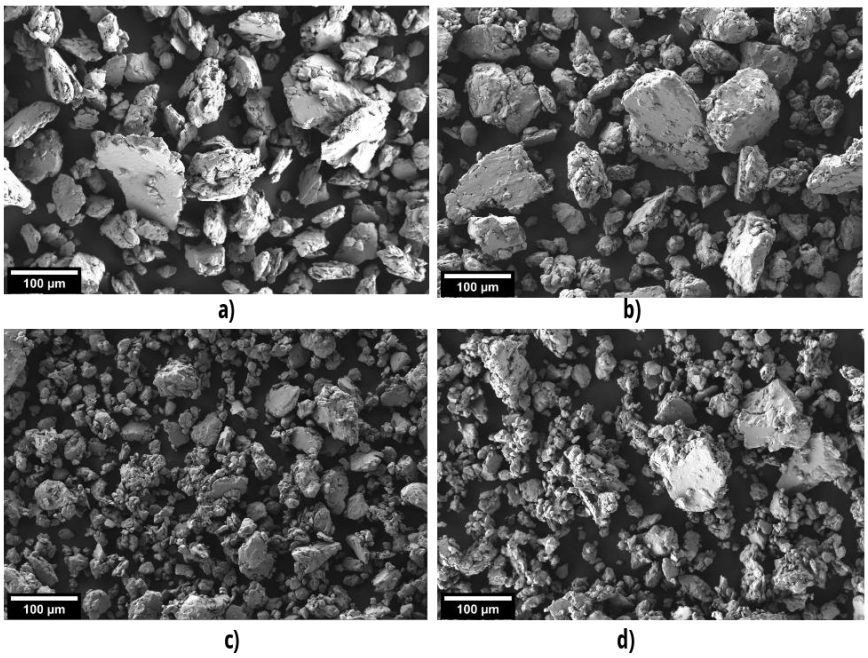

Fig. 3: SEM images of the material that passes the 100 μm sieve after different milling times. a) 2h, b) 5h, c) 10h and d) 20h

In EDS maps (see Fig S2, Supplementary material) it can be seen that part of the inhomogeneity of the starting material can still be observed after 2h of milling, with Mg and Al separated regions, but practically disappears after 5h.

3.2 Structural evolution of the milled material

Several structural changes are observed in the material as milling proceeds. The identified phases in the starting material are: a (Mg) solid solution, Al (PDF 00-004-0787), the intermetallic $Mg_{17}Al_{12}$ also known as β-phase (PDF 00-001-1128), and some residual MgO (PDF 00-045-0946). The (Mg) solid solution is characterized by a small shift in the diffraction peaks of pure Mg (PDF 00-035-0821) and is typically observed in Mg commercial alloys with Al as solute [Song]. As milling advances the amount of Al dissolved in (Mg) changes, Al peaks disappear, the amount of β-phase augments, and Fe peaks (PDF 00-006-0696) appear and slightly grow. Table 1 resumes the structural characteristics determined from Rietveld refinement of the data as a function of milling time (Fig. S3 in supplementary material shows a typical diffractogram and its refinement).

	Starting material	2h	5h	10h	20h
(Mg) [wt%]	88(2)	86(1)	90(2)	90(6)	78(4)
Al content in (Mg)* [at.%]	1.1(2)	1.6(2)	3.6(2)	6.7(2)	4.9(2)
Al [wt%]	4.9(2)	8.2(1)	2.4(3)	-	-
β-$Al_{12}Mg_{17}$ [wt%]	4.5(3)	2.1(1)	3.1(3)	4.4(5)	12(1)
MgO [wt%]	2.2(3)	3.9(1)	4.3(3)	4.7(6)	8.0(5)
Fe [wt%]	-	0.1(1)	0.4(1)	1.1(1)	2.3(1)
Refinement quality, Rwp [%]	4.5	3.5	3.0	3.7	2.7

* Al content was estimated using the relationship between lattice parameter and solubility of Al in (Mg) from [Murray 1982].

Table 1. Quantification of phases and structural characteristics of the materials from Rietveld refinement of diffractograms.

The amount of Al dissolved in (Mg) increases up to 10h of milling, and then slightly decreases. In all the cases the quantity of Al exceeds the equilibrium solubility reported in [Murray 1982] of 1.0 at% at 100 ºC. Solid solubility extensions beyond equilibrium by mechanical milling have been reported in many systems [Suryanarayana]. The fraction of metallic Al diminishes from 2h to 5h of milling, and after that, disappears. The reduction in the proportion of Al can be explained by a fraction being dissolved in (Mg) and another fraction contributing to the formation of β-phase, whose quantity monotonically increases with milling time. After 5h of milling a small amount of Fe can be quantified. The abundance of Fe increases with milling time and is attributed to contamination from the milling tools. It is interesting to note that milling under air does not produce a great amount of MgO. This is in agreement with the estimated amount of extra MgO of 1.8 wt%, expected from the oxidation of Mg by the oxygen contained in the milling chamber volume.

As milling proceeds crystallite size reduces and microdeformations accumulate in the material. Figure 4 shows the evolution of these quantities for (Mg), as determined from Rietveld refinement.

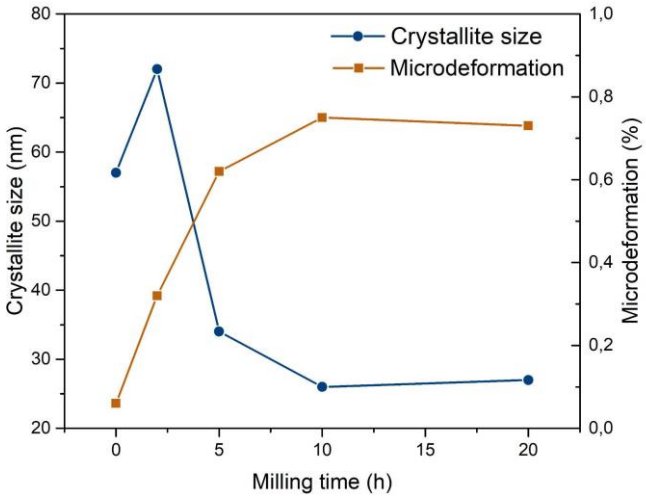

Fig. 4: Evolution of microstructure with millling time from Rietveld refinement of the XRD data.

It can be seen that the main microstructural modifications take place during the first 5 hours. After 2h microdeformations accumulate in the material and a small increase in crystallite size takes place. With 5h of milling crystallite size starts to decrease and microdeformations increase a bit more. Additional milling time does not produce substantial microstructural changes.

3.3 Hydrogen production by hydrolysis

The production of hydrogen by the hydrolysis reaction depends on size fraction and milling time. Due to the inhomogeneity of the 2h-milled material, only the results from the materials milled at least 5h are presented. Fig. 5 exemplifies the influence of size on the hydrolysis of the 5h-milled material (Figs. S4-S5 in the supplementary material completes the picture with the 10h and 20h-milled materials).

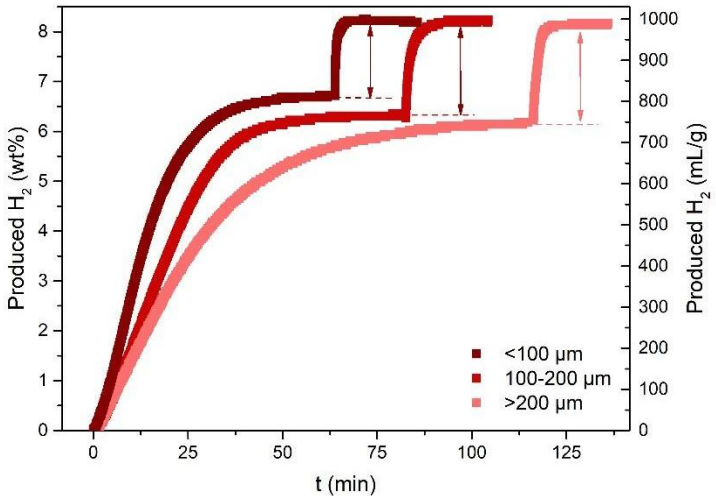

Fig. 5: Amount of H_2 produced as a function of time during the hydrolysis reaction of the different size ranges of the 5h-milled material. The jumps indicated by arrows correspond to the hydrogen released after acid addition.

Hydrogen release rates noticeably increase for smaller size ranges. Before acid addition the materials release a maximum amount of H_2 between 750 and 820 mL/g . Hydrogen release stops as a consequence of the formation of a layer of $Mg(OH)_2$ that prevents reaction. When acid is added, this layer is removed and total H_2 releases of the order of 1000 mL/g are observed. The maximum amount of H_2 expected for this material, assuming that Mg and Al are fully hydrolyzed is 1028 mL/g. Hence, yields of 73 – 80% and of 97 % are obtained before and after acid addition, respectively. The quotient between the amount of H_2 produced without acid and that obtained after acid addition can be considered as a practical yield. In this case, practical yields of the order of 75-82% are obtained.

The improvement of hydrogen production for longer milling times is illustrated in Fig. 6, for the size fraction in the 100 – 200 µm range (Figs. S6-S7 in the Supplementary material show the curves for the others size ranges).

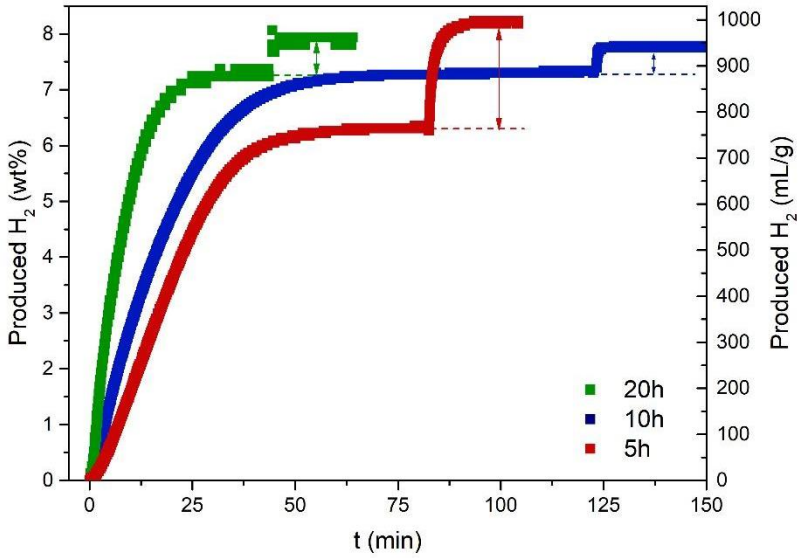

Fig. 6: Influence of milling time on the H_2 produced during the hydrolysis reaction of the material in the 100 – 200 µm size range.

It can be observed that the rate and amount of H_2 produced before acid addition increases for longer milling times. In this case the rate improvement cannot be attributed to a size effect, as the hydrolyzed material has been selected in the 100-200 µm range by sieving. Faster H_2 kinetics production are mainly due to the higher abundance of phases that form galvanic pairs with Mg, as it will be discussed below. It is also interesting to note that the practical yield increases with milling time, going from 78% to 94% when milling time increases from 5h to 10h or 20h.

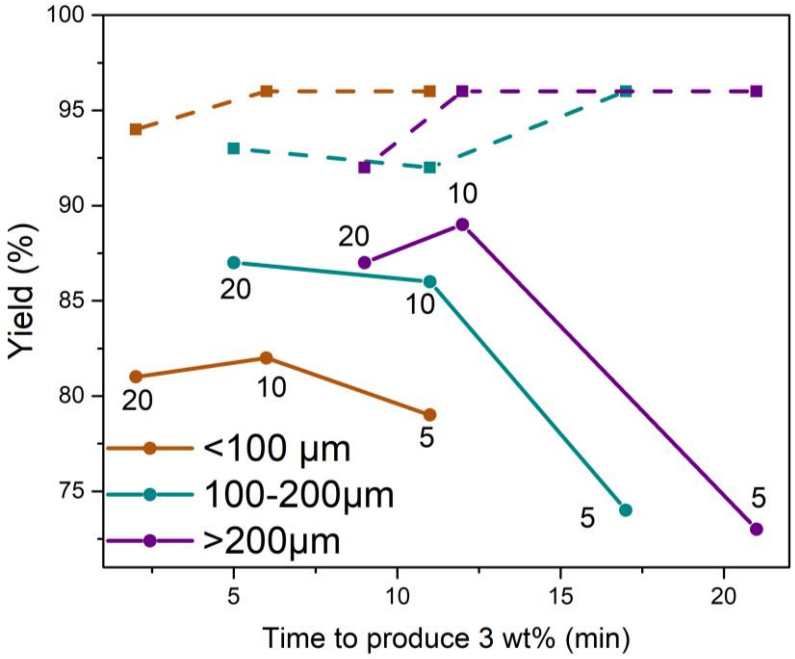

Fig. 7: Capacity and rate relationship for different size ranges and milling times. The absolute yields before (full line) and after (dashed line) acid addition are plotted as a function of the time needed to produce 3 wt% (364 mL/g) of H_2. The labels beside data points indicate milling time in hours.

The effect of particle size and milling time on the yield and the time taken to produce 3 wt% of H_2 (364 mL/g) is shown in Fig. 7 for all the studied materials (see also Table 2). By looking at the curves for each size range before acid addition, it can be seen that they move down and to the left as the size range decreases. This means that kinetics improves (i.e. less time is taken to produce a definite amount of H_2) but yields worsen with size reduction. A sort of compromise appears: smaller sizes mean faster kinetics, but also mean lower yields. The kinetic improvement can be linked with the decrease in agglomerates size and the changes in phase abundance, as it will be discussed below. The lower yields for smaller size ranges cannot be attributed to a lower amount of hydrolyzable material, since the yields after adding acid are similar. This trend suggests that the blocking of the hydrolysis reaction by the formation of a $Mg(OH)_2$ passivating layer occurs faster and is more effective in the smaller materials, leaving a larger fraction of unreacted, inaccessible Mg.

If attention is focused on each size fraction, better kinetics and yields are observed as milling time increases. The 100 – 200 μm size range is particularly interesting, since the size of the agglomerates in this case can be considered approximately uniform (Fig. 2). The increase in yield from 5h to 10h and 20h of milling seems to be due to the hydrolysis of part of the Al dissolved in (Mg) and/or part of the β-phase, as the observed yields exceed the expected values considering only the content of Mg in these materials (Table 2). The faster kinetics with milling time can be attributed to changes in phase abundance, as microstructure does not substantially change from 5h to 20h of milling (Figure 4). Table 1 shows that from 5 to 20h of milling the amounts of β-$Mg_{17}Al_{12}$ and Fe increase. According to [Song] $Mg_{17}Al_{12}$ can have a dual role in Mg corrosion, depending on the amount, distribution and most importantly the continuity of this phase. A continuous β-phase stops the development of corrosion by acting as a protective barrier, but a discontinuously distributed phase promotes hydrolysis by acting as micro-galvanic cathodes. The characteristic microstructure of a milled material favors a discontinuous distribution of β-$Mg_{17}Al_{12}$, hence a beneficial effect on hydrogen generation is expected. The presence of Fe also favors hydrolysis, due to its more positive electrochemical potential and the formation of galvanic couples between Mg and Fe. The effects of Fe on accelerating corrosion in Mg alloys are well-known [Song, Sevastyanova 2017]. Therefore, the combination of both contributions, related with the presence of Fe and β-$Mg_{17}Al_{12}$, is identified as the main cause of the improvement of hydrolysis kinetics.

Material	Yield (%)	Yield w/ acid (%)	3wt% time (min)	Expected yield (%) from Mg hydrolysis	Expected yield (%) from Al in (Mg) hydrolysis	Expected yield (%) from β-$Mg_{17}Al_{12}$ hydrolysis
5h < 100 μm	79(2)	96(4)	11	84(1)	+5(1)	+4(1)
5h 100 – 200 μm	74(2)	96(4)	17			
5h > 200 μm	73(2)	96(4)	21			
10h < 100 μm	82(2)	96(4)	6	84(1)	+9(1)	+5(1)
10h 100 – 200 μm	86(2)	92(4)	11			
10h > 200 μm	89(2)	96(4)	12			
20h < 100 μm	81(2)	94(4)	2	72(1)	+6(1)	+14(1)
20h 100 – 200 μm	87(2)	93(4)	5			
20h > 200 μm	87(2)	92(4)	9			

Table 2. Quantitative data from the hydrolysis curves of the studied materials. Columns 5-7 give expected yields calculated from phase abundances determined from Rietveld refinement of the XRD

data. Columns 6 and 7 give the additional increase in the expected yield of column 5 if Al dissolved in (Mg) is hydrolyzed or if β-$Mg_{17}Al_{12}$ is hydrolyzed, respectively.

Besides the kinetics – yield compromise discussed after Fig. 7, it is interesting to note that despite having processed the wastes by mechanical milling under air, yields without acid addition in the 80-90% range are obtained after milling 10 - 20h. The formation of a fraction of MgO only affects hydrogen production by excluding a small amount of Mg from being hydrolyzed, but does not apparently affect kinetics. To further explore this, hydrogen production from a sample of the 20h milled material stored for 1 year inside a vial closed under air was compared with that of a material stored 1 year under Ar inside the glovebox (Fig. 8).

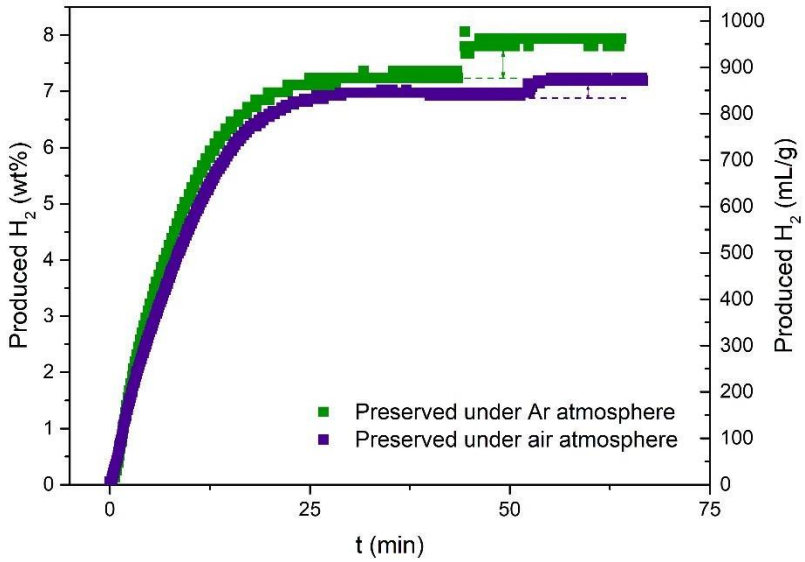

Fig. 8: Effect of exposure to air. Hydrogen produced from a 20h-milled material stored 1 year under Ar (green) and 1 year under air (purple). In both cases size is in the 100 – 200 μm range.

The only effect of the storage in air is a small reduction in the amount of H_2 produced and a little reduction in rate. The MgO film formed on the surface under air prevents the material from further oxidation, but does not avoid hydrolysis. According to [Song], the $Mg(OH)_2$ formed from the MgO layer after immersion in an aqueous solution has a porous structure that exposes fresh Mg and does not protect against corrosion.
To obtain some information about the kinetic mechanism during the hydrolysis reaction before acid addition, the shape of the hydrolysis curves was compared with that of various kinetic models described in [Khawam 2006]. As some of these models assume size uniformity, only the hydrolysis curves of the materials in the 100 – 200 μm range were examined. The analysis was done looking for linearity in the time dependence of the integral form of each kinetic model g(α), where α is the conversion fraction (more details can be found in the cited reference). Conversion fraction values in the 0.1 – 0.9 range were considered and only models with deceleratory reaction rates were taken into account.

Table 3 presents R^2, the square of the correlation coefficients of the linear fitting of g(α), and Fig. 9 shows the fitting and the difference between the measured data and the fitted model of the three best cases. In the left panel of Fig. 9 it can be seen that the geometrical contraction models give an excellent fit of the experimental curves. Correlation coefficients of 0.999 are obtained for all the milling times.

Interestingly, the best fit changes from contracting area model (R2) for 5h of milling to a contracting volume model (R3) for 10 and 20h of milling. This trend is consistent with the morphology of the milled materials shown in Fig. 2, in which flatter agglomerates are observed for grinding times of 2h and 5h, and more rounded agglomerates are seen as milling time increases. Therefore, it can be concluded that the hydrolysis reaction is controlled by the contracting area/volume of the particles, i. e. by the reaction interface progress towards the center of the agglomerates. These models consider that the rate limiting step is the speed of interface advance. This implies that the reactants arrival to this interface is not limited by diffusion through a product layer surrounding the particles. The results presented here show that this seems to be the case in the 0.1-0.9 conversion fraction range, where excellent fittings are obtained. For higher conversion fractions the blocking effect produced by the $Mg(OH)_2$ layer strongly affects kinetics, up to the point of stopping the reaction, as the need of adding acid to complete the reaction reveals.

Model	5hs	10hs	20hs
R2 (Contracting area)	0.999	0.997	0.999
R3 (Contracting volume)	0.996	0.999	0.999
D1 (1-D diffusion)	0.988	0.997	0.996
D2 (2-D diffusion)	0.967	0.990	0.982
D3 (3-D diffusion-Jander)	0.918	0.956	0.938
D4 (Ginstling-Brounshtein)	0.953	0.981	0.970
F1 (First order)	0.976	0.993	0.984
F2 (Second order)	0.832	0.878	0.848
F3 (Third order)	0.645	0.705	0.661

Table 3. Squared linear correlation coefficient of the linear fitting of g(α) vs. time for the different kinetic models considered. The best three values for each milling time are highlighted.

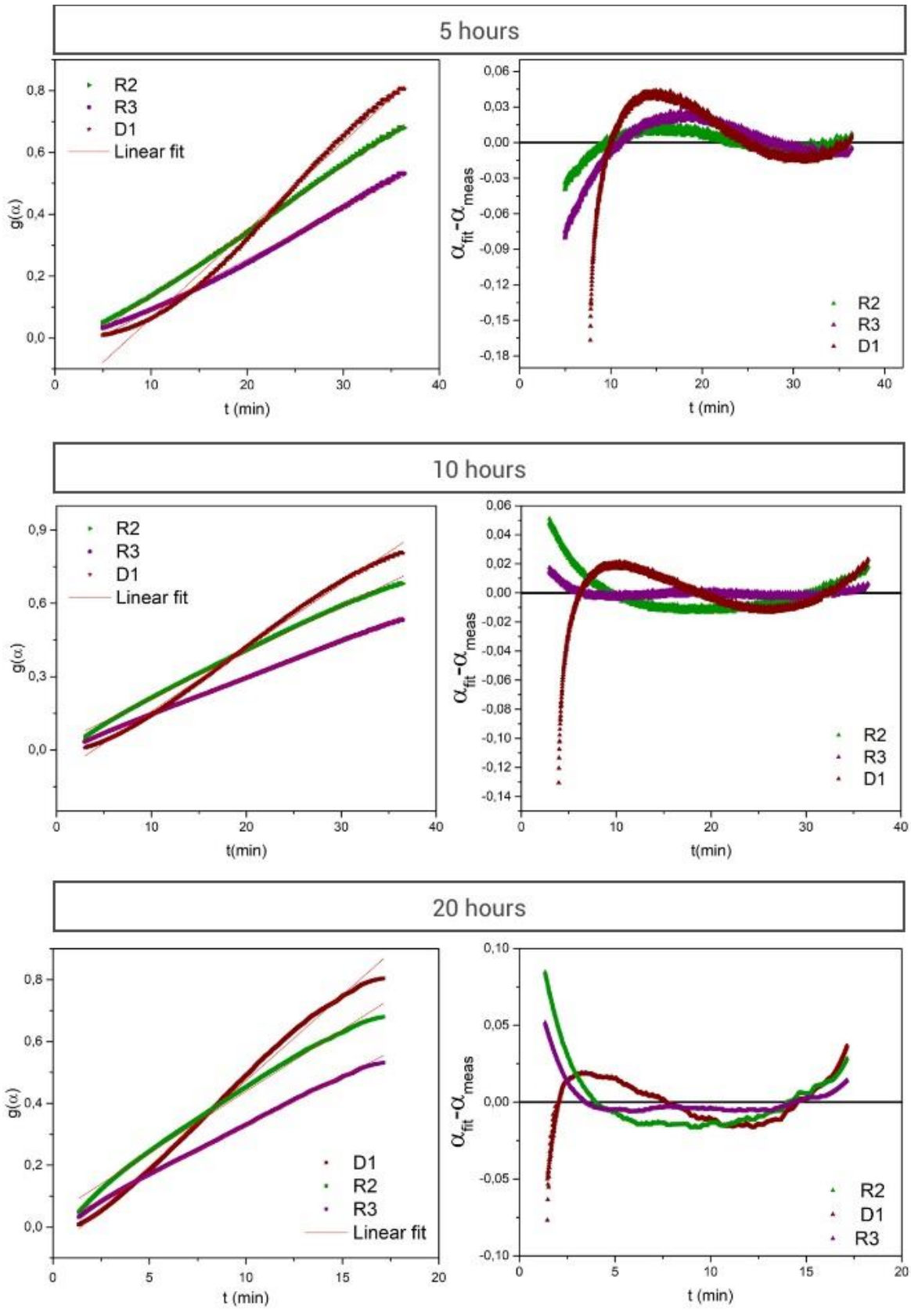

Fig. 9: Plots of g(α) vs. time (left) and differences between the measured α values and the fitted models (right) for 5, 10 and 20 h milling time.

From the fitting of the hydrolysis data the reaction rate constant can be determined. In the case of the R3 model its value increases with milling time from 2.05 10^{-4} s^{-1} to 2.50 10^{-4} s^{-1} and 5.24 10^{-4} s^{-1} for 5h, 10h and 20h, respectively. The rate constant of the R3 model is the quotient between the interface advance speed and the characteristic size of the particles [Khawam 2006]. The size uniformity of the 100 – 200 μm range materials (Fig. 2) allows attributing the increase in the rate constant to higher interface advance speeds due to the presence of Fe and β-phase, as previously discussed. Although the geometric contraction models have been identified as the best fitting models for the 100 – 200 μm size range materials, it is possible that volume contraction could be the rate limiting mechanism for the other size ranges too. The observation of faster rates for smaller size ranges at equal milling times (Fig. 7) is compatible with this idea. The non-systematic identification of a single rate limiting process for the < 100 μm and > 200 μm size ranges could be a consequence of lack of size uniformity.

Conclusions

Hydrogen was successfully produced by the hydrolysis of Mg-based wastes from the manufacturing of sacrificial anodes. Before hydrolysis, the scraps were reprocessed by mechanical milling up to 20h under air atmosphere without using expensive inert or reactive gases. Hydrogen yields in the 80 – 90% range were obtained after 30 minutes of reaction for materials milled at least 10h. The effects of oxidation during reprocessing were limited to a small loss of reactive material due to the formation of 4 – 8 wt. % of MgO.

Particle size strongly decrease, microstructural changes like crystallite size reduction and increase of microdeformation take place, and phase abundance changes during milling. Additionally, the incorporation of up to 2.3 wt% of Fe impurities from the milling tools and the formation of β – $Mg_{17}Al_{12}$ induce a positive effect on hydrolysis, as these phases accelerate the rate of hydrogen evolution by acting as micro-galvanic cathodes.

Reactants are not exhausted during the reaction in saline solution, due to the formation of a $Mg(OH)_2$ passivating layer. By adding HCl acid to the solution the reaction completes. Hydrogen production rate increases with milling time and with the decrease of the agglomerates size. However, size reduction has a negative side, as yield before acid addition decreases with size, suggesting that the $Mg(OH)_2$ blocking effect is stronger for small particles.

Storage of the milled materials under air does not impair its performance in hydrogen production by hydrolysis reaction.

By the shape of the hydrolysis curves a geometric contracting mechanisms R2 and R3 have been identified as the rate limiting processes during hydrolysis in the saline solution.

Acknowledgments

This work has been financially supported by CONICET (PIP 112 201501 00610), Universidad Nacional de Cuyo (06/C602) and MINCyT-ECOS-SUD (PA17A03). Bernardo Pentke is acknowledged for his assistance with the scanning electron microscope. Franco Niro and María Rodríguez acknowledge financial support from CNEA fellowships.

References

[Nikolaidis 2017] Nikolaidis P, Poullikkas A. A comparative overview of hydrogen production processes. Renew Sustain Energy Rev 2017; 67: 597-611.

[Mazloomi 2012] Mazloomi K, Gomes C. Hydrogen as an energy carrier: Prospects and challenges. Renew Sustain Energy Rev 2012; 16: 3024-3033.

[Abe 2019] Abe JO, Popoola API, Ajenifuja E, Popoola OM. Hydrogen energy, economy and storage: Review and recommendation. Int J Hydrogen Energy 2019; 44: 15072-15086.

[Xu 2018] Xu S, Liu J. Metal-based direct hydrogen generation as unconventional high density energy. Energy 2019; 13: 27-53.

[Marrero-Alfonso 2009] Marrero-Alfonso EY, Beaird AM, Davis TA, Matthews MA. Hydrogen generation from chemical hydrides. Ind. Eng. Chem. Res. 2009; 48: 3703-3712.

[Liu 2021] Liu Z, Zhong J, Leng H, Xia G, Yu X. Hydrolysis of Mg-based alloys and their hydrides for efficient hydrogen generation. Int J Hydrogen Energy 2021; 46: 18988-19000.

[Prasad 2021] Prasad SVS, Prasad SB, Verma K *et al.* The role and significance of Magnesium in modern day research-A review. J Mg Alloys in press. https:// doi.org/ 10.1016/ j.jma.2021.05.01

[Uan 2007] Uan J-Y, Cho C-Y, Liu K-T. Generation of hydrogen from magnesium alloy scraps catalyzed by platinum-coated titanium net in NaCl aqueous solution. Int J Hydrogen Energy 2007; 32: 2337-2343.

[Uan 2009] Uan J-Y, Lin M-C, Cho C-Y, Liu K-T, Lin H-I. Producing hydrogen in an aqueous NaCl solution by the hydrolysis of metallic couples of low-grade magnesium scrap and noble metal net. Int J Hydrogen Energy 2009; 34: 1677-1687.

[Uan 2009 b] Uan J-Y, Yu S-H, Lin M-C, Chen L-F, Lin H-I. Evolution of hydrogen from magnesium alloy scraps in citric acid-added seawater without catalyst. Int J Hydrogen Energy 2009; 34: 6137-6142.

[Figen 2015] Figen AK, Coşkuner B, Pişkin S. Hydrogen generation from waste Mg based material in various saline solutions ($NiCl_2$, $CoCl_2$, $CuCl_2$, $FeCl_3$, $MnCl_2$). Int J Hydrogen Energy 2015; 40: 7483-7489.

[Figen 2 2015] Figen AK, Filiz BC. Hydrogen production by the hydrolysis of milled waste magnesium scraps in nickel chloride solutions and nickel chloride added in Marmara Sea and Aegean Sea Water. Int J Hydrogen Energy 2015; 40: 16169-16177.

[Matsuzaki 2017] Matsuzaki K, Murakami T. Formation of Hydrogen by Ball Milling of Mg and Mg Alloy in Seawater. Mat Sci For 2017; 879: 1265-1269.

[Al Bacha 2019] Al Bacha S, Awad AS, El Asmar E, Tayeh T, Bobet J-L, Nakhl M, Zakhour M. Hydrogen generation via hydrolysis of ball milled WE43 magnesium waste. Int J Hydrogen Energy 2019; 44: 17515-17524.

[Al Bacha 2020] Al Bacha S, Pighin S, Urretavizcaya G, Zakhour M, Castro FJ, Nakhl M, Bobet J-L. Hydrogen generation from ball milled Mg alloy waste by hydrolysis reaction. J Pow Sources 2020; 479: 228711

[Al Bacha 2020 b] Al Bacha S, Pighin S, Urretavizcaya G, Zakhour M, Nakhl M, Castro FJ, Bobet J-L. Effect of ball milling strategy (milling device for scaling-up) on the hydrolysis performance of Mg alloy waste. Int J Hydrogen Energy 2020; 45: 20883-20893.

[Fullprof] Rodriguez-Carvajal J. Recent advances in magnetic structure determination by neutron powder diffraction. Phys B – Phys Cond Matter 1993; 192: 55-69.

[Pighin 2020] Pighin S, Urretavizcaya G, Bobet J-L, Castro FJ. Nanostructured Mg for hydrogen production by hydrolysis obtained by MgH2 milling and dehydriding. J Alloys Compd 2020; 827: 154000.

[Song] Song G-L, editor. Corrosion of magnesium alloys. Woodhead Publishing, UK; 2011, ISBN 9781845697082.

[Murray 1982] Murray JL. The Al-Mg (Aluminum-Magnesium) System. Bull Alloy Phase Diagrams 1982; 3: 60-74.

[Suryanarayana] Suryanarayana C. Mechanical Alloying and Milling. Marcel Dekker, USA; 2004, ISBN 082474103X.

[Sevastyanova 2017] Sevastyanova LG, Genchel VK, Klyamkin SN, Larionova PA, Bulychev BM. Hydrogen generation by oxidation of “mechanical alloys” of magnesium with iron and copper in aqueous salt solutions. Int J Hydrogen Energy 2017; 42: 16961-16967.

[Khawam 2006] Khawam A, Flanagan DR. Solid-State Kinetic Models: Basics and Mathematical Fundamentals. J Phys Chem B 2006; 110: 17315-17328.